Saturation effect of background temperature and aridity on vegetation phenological sensitivity to urban warming

Zhang Zhenzhen[1*#], Hu Xinxin[1#], Zhang Yongqi[1], Cui Shufen[2], Sun Liheng[3], Lin Xingwen[1], Wu Chaofan[1], Zhang Zhaoyang[1], Chen Yuanjian[1], Wen Qingqing[4]

[1]College of Geography and Environmental Sciences, Zhejiang Normal University, Jinhua 321004, China

[2]College of Business, Lishui University, Lishui 323200, China

[3]Faculty of Management, Universiti Teknologi Malaysia, Johor Bahru 81310, Malaysia

[4]The Administration Center of Jinhua Wucheng Nanshan Provincial Nature Reserve, Jinhua 321000, China

*** Correspondence: Zhang Zhenzhen (zhangzhen@zjnu.cn)**

[#] **These authors contributed equally to this work**

Societal Impact Statement

As cities grow and climates warm, the Urban Heat Island (UHI) effect increasingly alters urban ecosystems. This study analyzed 293 Chinese cities to reveal how baseline temperature and aridity shape vegetation's response to UHI. We found a "saturation effect," where UHI's impact weakens under certain background conditions. This helps explain why urban greening outcomes vary regionally. Our findings offer new insight into urban ecology and can support climate-smart planning, helping cities adapt more effectively and sustainably.

Abstract:

Quantifying how background temperature and aridity constrain phenological sensitivity to urban warming requires identifying critical thermal thresholds and

hydrological boundaries driving spatial heterogeneity. This study assessed urban warming effects on vegetation phenology across 293 Chinese cities during 2010–2020. Urban-rural disparities (ΔSOS, ΔEOS) and temperature sensitivity ($R_{t\text{-}SOS}$, $R_{t\text{-}EOS}$) were quantified using satellite metrics. Results showed urban heat islands advanced SOS by 12.06 days and delayed EOS by 9.86 days relative to rural areas. A non-linear saturation effect was detected: phenological sensitivity to urban warming peaked at 4 °C (spring) and 6 °C (autumn), and significantly weakened beyond sensitivity saturation thresholds of 12.5 °C (SOS) and 4 °C (EOS). Aridity acted as a negative regulator that weakened warming benefits across most aridity index (AI) ranges and reversed them within $1.4 < AI < 2.0$. Combined, LST and AI explained 75.05% and 76.21% of spatial variance in SOS and EOS responses, respectively. Conceptually, these findings challenge the linear paradigm of warming-driven phenological shifts by demonstrating finite physiological benefits of urban warming. Ecologically, this study highlights the coupled heat-aridity constraints on urban vegetation, providing key implications for climate-adaptive urban ecological planning.

Keywords: urbanization; heat island effect; vegetation phenological sensitivity; aridity index; land surface temperature; saturation effect

1. Introduction

Vegetation phenology, a critical aspect of ecosystem dynamics, exhibits significant sensitivity to the coupling of thermal and moisture variations (Badeck et al., 2004; Yu et al., 2003). While recent investigations have highlighted how urban warming precipitates an earlier start of the growing season (SOS) and a delayed end of the growing season (EOS), it is increasingly recognized that these responses are not solely temperature-driven but are fundamentally constrained by the background aridity of the locale. Thus, the phenological 'benefits' of the Urban Heat Island (UHI) effect must be evaluated through a dual lens of heat and water availability from the outset (Jeong et al., 2019). The cascading effects of these shifts extend beyond mere phenological alterations, contributing to a spectrum of ecological and environmental challenges (Zhou et al., 2016; Qiu et al., 2017; Ding et al., 2020).

However, the degree to which warming benefits phenological changes has been widely debated (Chmielewski & Rötzer, 2001; Ding et al., 2020; Yao et al., 2017). Urban environments offer a unique 'natural laboratory' for testing these phenological theories. Unlike experimental warming plots, the urban heat island (UHI) effect represents a sustained, large-scale warming scenario that has persisted for decades (Grimm et al., 2008). This allows researchers to observe long-term vegetation adaptation and identify thresholds that are difficult to capture in short-term manipulative experiments. Moreover, the vast geographic distribution of cities across climatic gradients provides a natural experimental framework to test how identical warming magnitudes (UHI) interact with varying background climates (Figure 1). Empirical evidence from the Northern Hemisphere consistently shows that cities in cold high-latitude regions exhibit more advanced SOS and delayed EOS in response to urban warming (Dallimer et al., 2016; Gazal et al., 2008; Jia et al., 2021; Li et al., 2021; Meng et al., 2020). While these studies offer valuable evidence regarding spatial heterogeneity, the non-linear dynamics of these responses—specifically, the saturation thresholds where urban warming benefits diminish, and how background aridity modulates these thresholds—remain inadequately quantified across climatic gradients. Identifying such thresholds is critical for predicting urban ecosystem stability under continuous global warming scenarios.

The magnitude of urban-induced phenological shifts is not uniform. Background climate heterogeneity constrains vegetation responses to additional urban warming: phenological advancements are strong in cold regions but weaken as baseline temperatures rise, implying that phenological sensitivity is a variable state conditioned by local thermal conditions. In ecology, the "saturation effect" describes that stimulus efficacy declines beyond a threshold, rooted in tolerance curve theory (Angilletta, 2009): organismal physiological functions increase with environmental drivers until reaching physiological saturation, beyond which no further enhancement occurs (Ketola & Kristensen, 2017). Plant physiological processes (photosynthesis, respiration, transpiration) do not increase linearly with temperature; they slow down or even decrease beyond a thermal threshold (Sage & Kubien, 2007; Ge et al., 2021).

A meta-analysis has proved greater positive growth responses to warming in colder ecosystems (Rustad et al., 2001; Büntgen et al., 2019). We therefore hypothesize that urban warming benefits for phenology (advanced SOS, delayed EOS) gradually approach saturation in warmer regions, and extra UHI warming will no longer promote phenological shifts. This theory remains to be verified in urban phenology systems.

It is noteworthy that drought conditions adversely disrupt temperature-driven phenological responses (Peng et al., 2019; Yuan et al., 2020). Urban vegetation is more vulnerable to moisture deficits due to the 'Urban Dry Island' effect (reduced soil moisture and elevated evaporation in built environments) and impervious surfaces (Zhang et al., 2019). UHI warming combined with high aridity elevates vapor pressure deficit and water demand, triggering defensive mechanisms (e.g., ABA accumulation (McAdam, 2013), protein degradation) that offset thermal advancements. Drought delays spring SOS and advances autumn EOS by inducing water stress and early dormancy (McAdam, 2013; Čehulić et al., 2019). However, in urban environments, this drought effect is compounded by the Urban Dry Island and impervious surfaces, further attenuating phenological sensitivity to extra warming, diminishing the positive impacts of UHI; this effect is stronger in warmer cities where plants approach thermal limits.

Consequently, we hypothesize that background aridity (AI) acts as a critical negative regulator of the thermal saturation threshold. Specifically, we predict that as background aridity increases, the 'saturation point' at which warming benefits (such as advanced SOS or delayed EOS) plateau will occur at lower LST values. This implies that the saturation effect is not a fixed thermal threshold but a dynamic state conditioned by water stress, leading to a more rapid decline in phenological sensitivity in arid urban environments.

Furthermore, phenological sensitivity to environmental drivers is species-specific and modulated by functional traits. Broad-leaf and coniferous species show divergent responses to warming and drought due to differences in leaf morphology and hydraulic architecture (Zheng et al., 2022). However, whether the 'saturation effect'

and 'aridity-driven inhibition' operate consistently across urban vegetation types remains unclear.

As a rapidly urbanizing country with diverse climates, China faces severe UHI challenges (He et al., 2017). UHI intensity averages 0.9 ± 1.1 ℃ but varies drastically across regions (Li et al., 2021).Previous urban phenology studies focused on linear temperature sensitivity, ignoring nonlinear saturation effects and the interactive regulation of aridity. No study has quantified critical thermal/arid saturation thresholds, nor clarified the coupling mechanism between preseason temperature (T, phenological sensitivity) and land surface temperature (LST, background climate) in urban ecosystems. China's large climatic gradients and rapid urbanization make it an ideal platform to test the saturation hypothesis and aridity modulation.

Thus, an investigation into the phenological response of plants to urbanization in China would enhance our understanding of their ability to acclimate to climate changes across various environments. However, how background temperature and aridity interactively determine the thresholds and 'saturation' of phenological sensitivity to urban warming remains largely unquantified at a macro-scale. Addressing this gap is essential for predicting the stability of urban carbon sinks under future climate scenarios. To this end, the primary objectives of this study encompassed the following: (1) explore the spatial distribution of plant phenological responses to the urban heat island effect throughout mainland China; (2) quantify the saturation effect caused by the spatial variability of phenological responses correlated with background temperature across the cold-hot gradient; and (3) assess whether the benefits of urban warming would be counteracted in drought-affected areas.

2. Materials and Methods

2.1 Study area

In our study, we conducted an analysis covering a total of 293 prefecture-level cities in China (excluding Taiwan, Autonomous Prefecture, and regions), taking into account the data from the year 2020 (http://xzqh.mca.gov.cn/map) (Figure 1). It was hypothesized that the urban warming effect is most pronounced in urban centers and

gradually diminishes towards rural areas (Zhang et al., 2004). To determine the urbanization intensity of each city, nighttime light data from NPP-VIIRS (Table 1) was utilized (Elvidge et al., 2017), employing the reference comparison method. The optimal segmentation threshold was established based on the statistical yearbook (Fan et al., 2019). Moreover, urban built-up areas were identified using the comparison method and annual average data derived from NPP-VIIRS night lights between 2013 and 2020. All data processing procedures were performed using ArcGIS 10.2. A total of ten buffer zones were created within a radius of 20 kilometers from the city center, with each buffer zone set at a distance of 2 kilometers from the center (Figure 1).

This specific 20 km delineation was established because our preliminary analysis revealed that the urban warming footprint on phenological metrics (SOS and EOS) gradually diminishes and approaches zero at distances of 15 km and beyond (Zhang et al., 2004; Figure 1, Figure 2). Thus, defining the outermost 20 km buffer zone as the "Rural" baseline guarantees a background environment conservatively free from urban heat island interferences. The subscript "(10)" used throughout this manuscript refers to the 10-th buffer zone located 20 km away from the urban center, and all notations in equations have been standardized to use buffer index (0 for urban center, 10 for rural reference) to avoid misinterpretation between distance and buffer number.

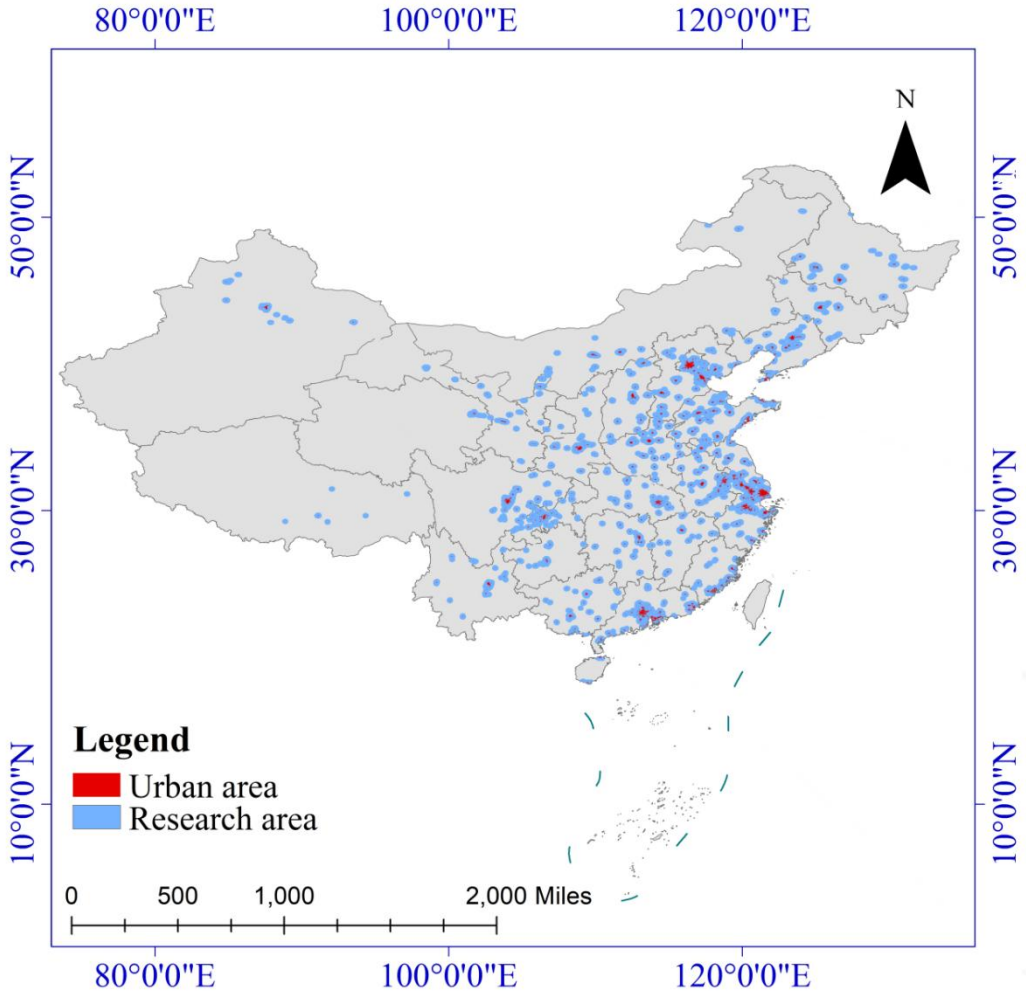

Figure 1. City centers (red area) and buffer zones (blue area) of the 293 prefecture-level cities in China. The map, generated using ArcGIS – version 10.2 (https://www.esri.com/about/newsroom/arcwatch/the-best-of-arcgis-10-2/), features administrative boundaries sourced from the Ministry of Civil Affairs of the People's Republic of China (http://xzqh.mca.gov.cn/map). Source: Esri, TomTom, FAO, USGS, and the GIS User Community; Ministry of Civil Affairs of the People's Republic of China | Powered by Esri.

2.2 Vegetation phenology extraction

Phenology data spanning the years 2010 to 2020 were derived from MODIS Enhanced Vegetation Index (EVI) 16-day composite data with a spatial resolution of 250 m (MOD13Q1) and processed utilizing TIMESAT (Jönsson & Eklundh, 2004). To mitigate challenges such as cloud cover and snow, the raw EVI time series data were smoothed using the Savitzky-Golay (S-G) filter method (Cai et al., 2017).

Subsequently, a dynamic threshold technique was employed to extract the phenology data, utilizing a seasonal amplitude of 20%, a parameter proven effective for phenology extraction in urban environments (Zhou et al., 2016; Buyantuyev & Wu, 2012; Cong et al., 2012; White et al., 2009). The datasets underwent preprocessing and quality control to eliminate pixels with minimal vegetation EVI (e.g., bodies of water and fully paved surfaces). To exclude unrealistic phenological values, we retained only SOS (30–180 days) and EOS (210–360 days) within valid ranges, consistent with previous studies (Zhang et al., 2006). Efforts were made to reduce the impact of outlier years by averaging the phenology data for each pixel across the timeframe from 2010 to 2020. After applying these quality control thresholds and land-cover filtering criteria, approximately 48.5% of the initial pixels within the study buffer zones were excluded.

Furthermore, we employed land cover data from the MCD12Q1 dataset, which has a 500-meter resolution, to mitigate the impact of agricultural practices on the mainland during our analysis. The MCD12Q1 dataset categorizes land into 17 distinct classes. These include various types of forested areas such as Evergreen Coniferous Forests, Deciduous Needle-leaf Forests, Evergreen Broad-leaf Forests, Deciduous Broad-leaf Forests, Mixed Forests, as well as Closed Shrub lands, Open Shrub lands, Savannas, Woody Savannas, Grasslands, and Croplands.

Given the frequent human-induced disturbances in Croplands in the rural regions and the regular manual pruning of Grasslands in the urban center, Savannas, woody savannas, Grasslands, and Croplands were excluded from our study. The remaining land types were consolidated into broader categories: broad-leaf forests (BF, deciduous and evergreen broadleaf forests), coniferous forests (CF, deciduous and evergreen coniferous forests), mixed forests (MF), and shrubs (closed and open shrublands). This classification approach allowed us to focus our analysis on land types that are less influenced by human activities.

Table 1. Data inventory used in this study

Data type	Resolution	Layer	Data sources	Year
MOD13Q1	250m/16d	EVI	https://search.earthdata.nasa.gov	2010-2020

MOD11A2	1000m/8d	LST_Day LST_Night	https://search.earthdata.nasa.gov	2010-2020
MOD16A2	500m/8d	PET	https://search.earthdata.nasa.gov	2010-2020
MCD12Q1	500m	Land Cover	https://search.earthdata.nasa.gov	2010-2020
VIIRS	500m	yearly average	https://eogdata.mines.edu	2013-2020
Precipitation data	1000m	monthly average	http://www.geodata.cn	2010-2020
China's urban zoning data			https://www.resdc.cn	2020
Station climates		monthly average	http://data.cma.cn/en	2010-2020

2.3 Pre-season temperature and background climates

Building upon the methodology of a previous study (Piao et al., 2006), preseason temperature (T) was characterized as the mean temperature for the three months preceding the onset of the phenological season. For alignment with the phenology information, the average temperature dataset was resampled to a 250 m resolution using the nearest neighbor interpolation technique. To evaluate the performance of the downscaling procedure, the observed long-term monthly temperature and precipitation across China were obtained from the National Meteorological Information Center of China (http://data.cma.cn/en). This dataset included observations from 496 national weather stations during 2010–2020. Upon conducting a fitting analysis with station data, we observed that the coefficient of determination (R^2) for monthly mean temperature and remote sensing data reached 0.93, while that for monthly precipitation and remote sensing data achieved 0.85. These results indicated that the downscaled meteorological data sufficiently meet the requirements of this study.

The background climates were evaluated utilizing land surface temperature (LST) and the aridity index (AI) as indicators. The LST and AI data for each pixel were averaged over 2010 - 2020. Specifically, MODIS LST datasets exhibiting an absolute bias of less than 1K were selected as optimal for our investigation, in line with

previous studies (Gow et al., 2016; Pablos et al., 2016; Qiao et al., 2013; Wan et al., 2008). Collection 6 LST products from the Aqua satellite (MOD11A2, 8-day composite, 1km spatial resolution, covering the period from 2010 to 2020) were used. Additionally, daily temperature (T) was calculated as the mean of daytime and nighttime temperatures, following the methodology outlined by Kang (Kang et al., 2016). AI was expressed as:

$$AI = PET/P \quad (1)$$

where PET denotes the annual potential evapotranspiration and P denotes the annual precipitation. The PET values spanning from 2010 to 2020 were extracted from the MOD16A2 monthly synthetic product, characterized by an 8-day temporal resolution and a spatial resolution of 500 m (Mu et al., 2011), as delineated in Table 1. The annual precipitation (P) dataset was derived from the monthly precipitation records of China encompassing the timeframe from 1901 to 2020, possessing a spatial resolution of 1 km. Subsequently, both PET and P datasets were resampled to a spatial resolution of 250 m to facilitate the ensuing spatial analysis (Peng, 2020).

To robustly quantify these responses, we clarify the distinct analytical roles of two critical thermal dimensions: preseason air temperature (T) and land surface temperature (LST). In this study, T and LST serve strictly distinct analytical roles. Pre-season air temperature (T) is the direct biological driver of plant physiology (e.g., chilling requirements). Therefore, T is used exclusively to quantify the pure biological phenological sensitivity (Rt) and identify true physiological thresholds. Conversely, Land Surface Temperature (LST) is the standard metric for quantifying the Urban Heat Island (UHI) effect. Thus, LST is used to characterize the spatial 'background climate' of each city across the continent.

Because pre-season air temperature (T) is the direct driver of phenological sensitivity, we first derived the biological thresholds using T (Figure 5). However, to address our core objective—understanding how the background temperature (LST) determines these phenological shifts—we needed to clarify the quantitative relationship between the background LST and T. We fitted the relationship curve between LST and T across all cities. To strictly prevent data matching biases during

this conversion, we utilized the spatiotemporally aligned 10-year climatological means (2010–2020) for both variables at a unified 250-m resolution. We observed a highly robust linear correlation (Figure S4). Based on this high goodness-of-fit, we utilized the empirical conversion formula between the two variables to mathematically substitute T with LST in the sensitivity curves (Wan et al., 2008). This empirical translation allowed us to systematically convert the T-driven physiological thresholds into the specific LST-determined background climate thresholds (12.5 ℃ for SOS and 4 ℃ for EOS), explicitly projecting pure biological limits onto the urban map. While T and LST represent different physical properties, they are highly correlated in urban settings (R^2 = 0.93 for monthly mean temperature), ensuring the reliability of this empirically driven translation between physiological response and climatic background.

2.4 Urbanization effect on phenology

The phenology date of each vegetation was extracted in each buffer zone. Finally, the mean phenology in this buffer zone was weighted by the phenology of each vegetation type. To ensure comparability in phenological analyses across buffer zones, we first identified the common vegetation types present in all zones and excluded the non-shared ones. We then calculated the phenological means for these common types within each buffer zone and averaged these values to determine the overall mean vegetation phenology for the entire buffer region, as shown below (equation 2, 3).

$$SOS_i = \sum SOS_{ij} \Big/ n \quad (2)$$

$$EOS_i = \sum EOS_{ij} \Big/ n \quad (3)$$

SOS_i and EOS_i are the mean SOS and EOS of i-th buffer zone, SOS_{ij} and EOS_{ij} are the mean SOS and EOS of the j-th vegetation type in the i-th buffer zone; n is the number of the shared vegetation types in all the buffer zone.

To investigate the impact of urbanization on phenology, mean values of start of season (SOS) and end of season (EOS) in each buffer zone were analyzed for the period between 2010 and 2020, and fitted with respect to their distance from the urban center. In this study, the outermost buffer zone (20 km from the city center) was

defined as the rural reference region, and the city center was defined as the urban region. This delineation was justified by the observation that phenological change rates approached zero at 15 km and beyond (Figure S1), and similar patterns were observed for all four vegetation types (Figure S2). As per prior investigations, the phenological sensitivity (R_t) to temperature was quantified by calculating the partial correlation coefficient between T and the phenology dates ($R_{t\text{-}SOS}$ and $R_{t\text{-}EOS}$) (Meng et al., 2020). The phenological difference between urban and rural regions was calculated to quantify the magnitude of the urban warming effect on phenology:

$$\Delta SOS = SOS_{(0)} - SOS_{(10)} \quad (4)$$

$$\Delta EOS = EOS_{(0)} - EOS_{(10)} \quad (5)$$

Among which, $SOS_{(0)}$ and $SOS_{(10)}$ are the mean SOS of the urban center (buffer index 0) and the 10th buffer zone (located 20 km away), respectively. Similarly, $EOS_{(0)}$ and $EOS_{(10)}$ are the mean EOS of the urban center and the 10th buffer zone. Biologically, a negative ΔSOS value indicates an advanced start of the season (spring) in the urban center relative to the rural area, whereas a positive ΔEOS value signifies a delayed end of the season (autumn senescence) in the urban center.

Similarly, the difference in phenological sensitivity to temperature between urban and rural regions was defined as:

$$\Delta R_{t-SOS} = R_{t-SOS(0)} - R_{t-SOS(10)} \quad (6)$$

$$\Delta R_{t-EOS} = R_{t-EOS(0)} - R_{t-EOS(10)} \quad (7)$$

Among which, $R_{t\text{-}SOS(0)}$ and $R_{t\text{-}SOS(10)}$ are the mean $R_{t\text{-}SOS}$ of the urban center (buffer index 0) and the 10th buffer zone (located 20 km away), respectively. Similarly, $R_{t\text{-}EOS(0)}$ and $R_{t\text{-}EOS(10)}$ are the mean $R_{t\text{-}EOS}$ of the urban center and the 10th buffer zone.

2.5 Background climates determined phenology response

In order to elucidate the distinct impacts of LST and AI on urban and rural components, a partial correlation analysis was executed. Specifically, the average LST or AI values recorded from 2010 to 2020 for each of the 293 cities were correlated with their respective ΔSOS, ΔEOS, $\Delta R_{t\text{-}SOS}$, and $\Delta R_{t\text{-}EOS}$ values, while controlling for the influence of the other climatic factor.

This study employed path analysis (PA) as a methodological approach (Doncaster, 2007) to examine both the direct and indirect effects of background climate variables (LST and AI) on phenological responses (SOS and EOS), as well as their corresponding discrepancies (ΔSOS and ΔEOS) and rates of change ($\Delta R_{t\text{-}SOS}$ and $\Delta R_{t\text{-}EOS}$).

In the path analysis, we initially ascertained the model's congruence with empirical data by evaluating fit indices, including the chi-square (χ^2) statistic, Comparative Fit Index (CFI), and Root Mean Square Error of Approximation (RMSEA). Subsequently, path coefficients were derived for both the direct and indirect effects of each independent variable on the dependent variable from the model. The squared path coefficients for the direct and indirect paths estimated the respective direct and indirect contribution degrees of each independent variable to the dependent variable. The aggregate of these direct and indirect contribution degrees constitutes the total contribution degree, or relative contribution.

2.6 Validation of phenology "saturation effect"

To determine if there was a temperature saturation effect on vegetation phenology, we conducted a comparative model comparison. Rather than assuming a single relationship a priori, we evaluated the fit of phenology versus pre-season temperature using competing models: a linear model, a quadratic model, a segmented (piecewise) model, and a logistic model. We specifically selected the logistic function as our primary model because quadratic models biologically imply a symmetric reversal (a continuous steep decline) rather than a plateau, and piecewise models assume an abrupt, angular change in biological rates, which is less physiologically realistic than the smooth, asymptotic transition captured by the logistic curve (Pinheiro & Bates, 2000). The asymptote of the logistic function mathematically represents the biological 'saturation point'—the maximum physiological limit of thermal benefits.

Statistically, the model comparison results (Table 2) confirm that the logistic

model consistently outperforms the other three formulations for both spring SOS and autumn EOS, providing quantitative support for the nonlinear saturation effect interpretation. For SOS, the logistic model yields an AIC value 278 units lower than the linear model and 1424 units lower than the piecewise model, along with an R^2 of 0.37, which is approximately 19% higher than the second-best piecewise model. For EOS, the logistic model still achieves the lowest AIC and highest R^2, but the performance improvement is more modest: its R^2 (0.40) is only marginally higher than that of the piecewise model (0.39), consistent with a weaker but stable saturation pattern.

Table 2. Performance comparison of four competing models describing phenological responses to preseason temperature

Phase	Model	AIC	BIC	R^2	RMSE
Spring_SOS	Linear	104203.62	104218.97	0.25	26.52
	Quadratic	103636.33	103659.35	0.27	26.05
	Piecewise	102849.67	102880.36	0.31	25.41
	Logistic	101425.33	101456.02	0.37	24.29
Autumn_EOS	Linear	93252.94	93268.34	0.23	17.39
	Quadratic	90241.5	90264.6	0.36	15.86
	Piecewise	89309.4	89340.2	0.39	15.41
	Logistic	85678.49	85709.14	0.40	15.22

We then extracted phenological information from all vegetation pixels across the country and plotted scatter diagrams of phenology versus preseason temperature. Next, we fitted logistic growth curves to these scatter plots and evaluated the assumption using the goodness-of-fit metrics p-value and R^2. Subsequently, we applied the same logistic curve to characterize the phenological responses of urban and suburban vegetation in 293 different cities against their preseason temperatures, testing whether the phenological response to temperature in urban areas also follows a logistic growth pattern. Finally, we replaced the preseason temperature with the background temperature LST to determine how the phenological saturation effect is regulated by

the background temperature.

3. Results

3.1 Spatial distribution of urban-rural phenological differences

Among the 293 cities analyzed, 84% (N = 246) exhibited an advanced SOS in urban areas compared to rural regions, while 82% (N = 241) experienced a delayed EOS (Figure S3). Spatially, cities located in high-latitude regions generally demonstrated more negative ΔSOS values than those in low-latitude regions (Figure 2), indicating more advanced spring phenology in urban areas of high-latitude cities, which suggests a stronger impact of urban warming on SOS in Northern and Western China (Figure 2a, b). This pattern is consistent with the conventional understanding of earlier SOS in colder regions. Additionally, cities in coastal provinces exhibited larger ΔSOS values than inland cities (Figure 2).

A strong positive correlation was observed between ΔSOS and the rural rate of SOS change ($R_{t\text{-}SOS}$), suggesting that cities with more negative $R_{t\text{-}SOS}$ values exhibit larger urban-rural disparities (Figure 3). Notably, cities with lower temperatures tended to have more negative $R_{t\text{-}SOS}$ and ΔSOS distributions.

ΔEOS also showed a significant increasing trend with latitude gradient (Figure 2), with northern cities displaying more positive ΔEOS values, indicating a delayed autumn phenology in urban areas (Figure 2c, d). In contrast, the majority of cities in southern regions demonstrated negative ΔEOS values, signifying an advancement in autumn phenology. Furthermore, cities in the coastal provinces also exhibited larger ΔEOS values.

Similarly, when ΔEOS was analyzed in relation to rural rate of EOS change ($R_{t\text{-}EOS}$), a positive correlation was observed. Positive and negative ΔEOS values were predominantly found in cold and warm regions, respectively (Figure 3). Moreover, when $\Delta EOS > 0$, both the absolute value of ΔEOS and $\Delta R_{t\text{-}EOS}$ increased with temperature, while for $\Delta EOS < 0$, the absolute value of ΔEOS and $\Delta R_{t\text{-}EOS}$ decreased with temperature.

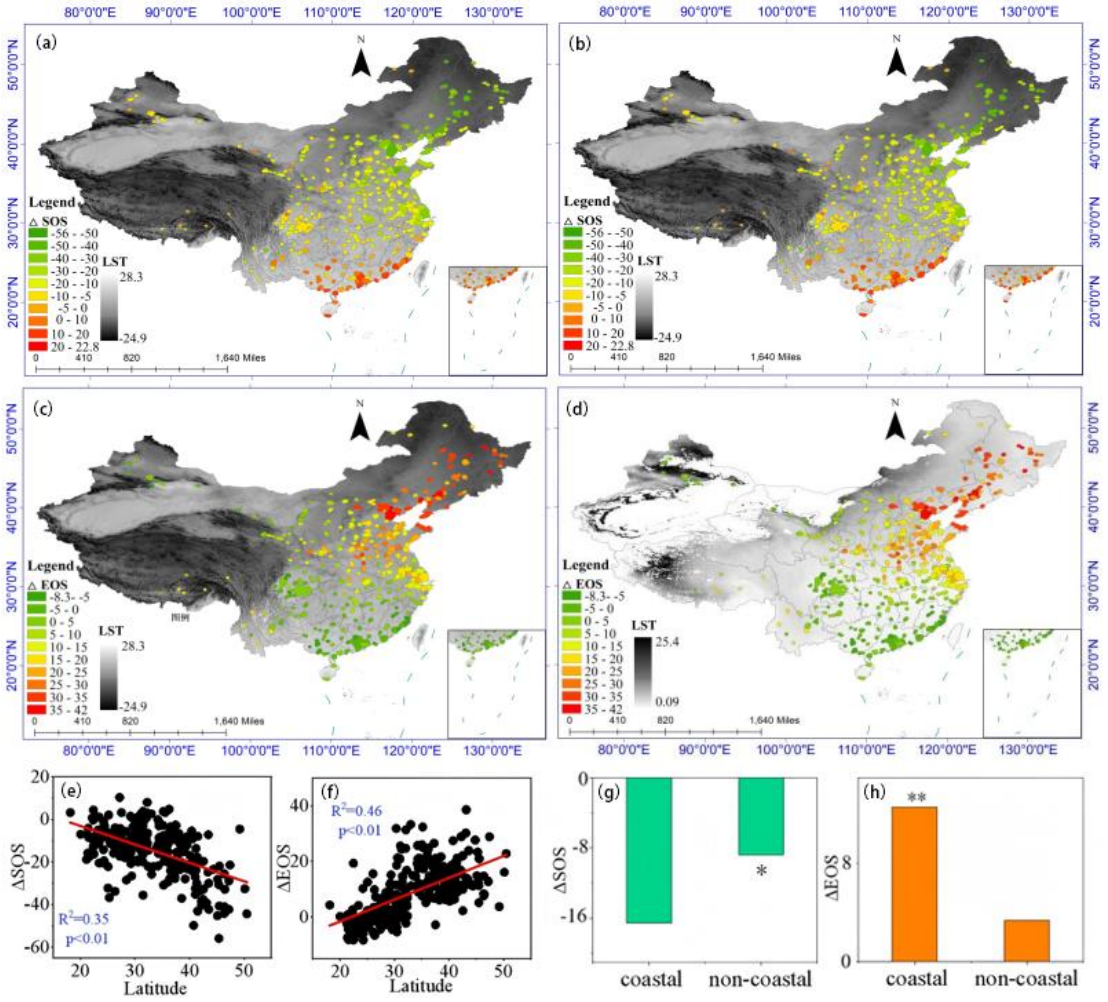

Figure 2. The spatial distribution of urban-rural disparities for SOS (ΔSOS) (a and b), EOS (ΔEOS) (c and d) was analyzed across mainland China. Mean land surface temperature (LST) was represented in black-and-white range for the entire continent, and the data in these figures reflected the 10-year mean from 2010 to 2020 for each city.

Panel (e) depicts the linear correlation between ΔSOS and latitude (R^2=0.35, p<0.01); panel (f) depicts the linear correlation between ΔEOS and latitude (R^2=0.46, p<0.01); panel (g) compares ΔSOS between coastal and non-coastal provinces (*p<0.05); panel (h) compares ΔEOS between coastal and non-coastal provinces (**p<0.01). The map, generated using ArcGIS – version10.2, features administrative boundaries sourced from the Ministry of Civil Affairs of the People's Republic of China (http://xzqh.mca.gov.cn/map). Source: Esri, TomTom, FAO, USGS, and the GIS User Community; Ministry of Civil Affairs of the People's Republic of China | Powered by

Esri.

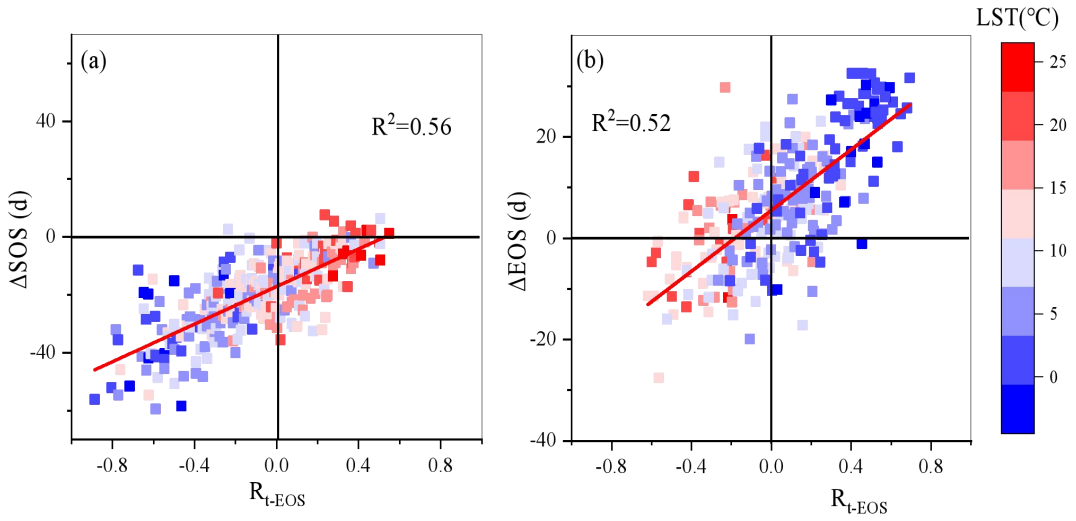

Figure 3. Relationship between urban-rural phenological difference and temperature sensitivity across 293 Chinese cities.

(a) Urban-rural difference in start of growing season (ΔSOS) versus temperature sensitivity of SOS ($R_{t\text{-}SOS}$).

(b) Urban-rural difference in end of growing season (ΔEOS) versus temperature sensitivity of EOS ($R_{t\text{-}EOS}$).

Each point represents one of the 293 cities analyzed, colored by land surface temperature (LST, ℃). Red solid lines indicate linear regression fits.

3.2 Phenology response to LST

As we compared urban and rural regions, logistic trends were observed for both SOS and EOS in relation to LST (Figure 4). In urban areas where LST was below 12 ℃, the SOS occurred notably earlier compared to rural regions, while urban areas exhibited a delayed EOS when LST was below 18.5 ℃. As LST decreased, the SOS stabilized at 101.3 days for urban regions and 129.7 days for rural regions, while the EOS stabilized at 321.3 days for urban areas and 310.8 days for rural areas. Conversely, when LST exceeded the specific thresholds for urban-rural differences (LST = 18 ℃ for ΔSOS and LST = 18.5 ℃ for ΔEOS), the phenological disparities between urban and rural areas were no longer significant and sometimes even

reversed (Figure 4a,b). As LST increased, the urban and rural SOS stabilized at 71.7 days (Figure 4a), and the urban and rural EOS stabilized at 327.4 days and 332.4 days, respectively. Fitting curve of ΔSOS and ΔEOS with LST revealed a positive and negative relationship, respectively, intersecting at LST = 18 ℃ and 18.5 ℃, indicating a shift in SOS and EOS dynamics with increasing temperatures beyond these thresholds.

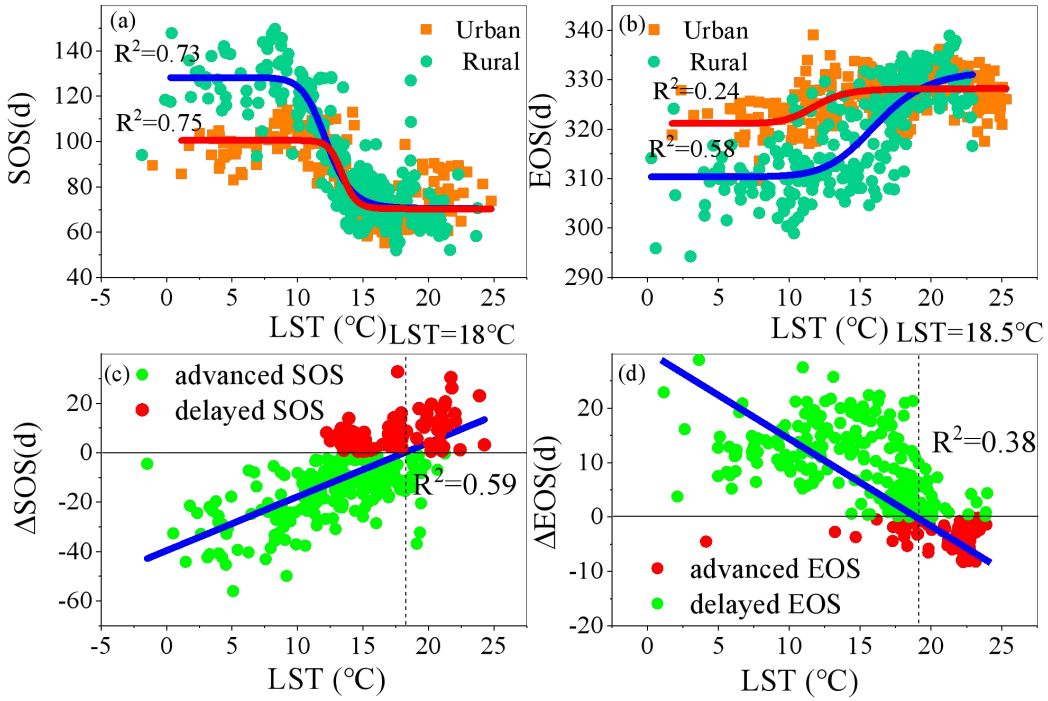

Figure 4. Relationship between background temperature (LST) and phenology (SOS and EOS) across the urban-rural regions (a, b) from 2010 to 2020, and the relation between ΔSOS and ΔEOS with the LST (c,d).

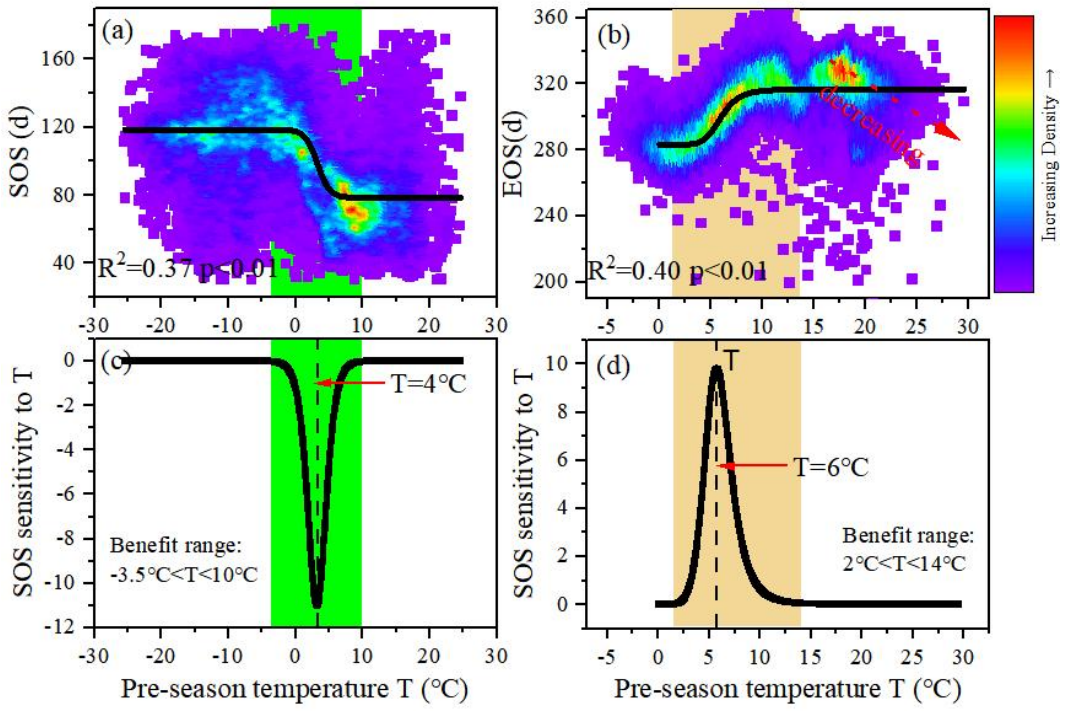

425

426 **Figure 5.** The relationship between preseason temperature (T) and SOS/EOS (a, b) as
427 well as their first-order derivatives (implying the phenological sensitivity to T) of the
428 fitting curve.

429 To determine whether the temperature sensitivity influenced the logistic trends of
430 phenology with LST, we conducted a nationwide fitting of phenology to T and also
431 derived logistic curves for SOS and EOS (Figure 5). The first-order derivatives of the
432 fitting curve that represented the phenological sensitivity to T revealed warming
433 benefits on SOS and EOS, ranging from -3.5 to 10℃ and 2.0 to 13.5℃, respectively.
434 The highest sensitivity was observed at T = 4 ℃ for SOS and T = 6 ℃ for EOS.
435 Notably, a decreasing trend for EOS was observed when T > 15 ℃, corresponding to
436 the advanced EOS when T > 18.5 ℃ (Figure 5d).

437 To assess the temperature sensitivity of phenological variations between urban
438 and rural settings across vegetation types, we established regression models for ΔSOS,
439 ΔEOS, and LST for each type (Figure 6). Findings revealed that shrublands had the
440 highest temperature sensitivity for both metrics, whereas CF displayed the lowest.
441 The temperature response of MF and BF showed no significant variation.

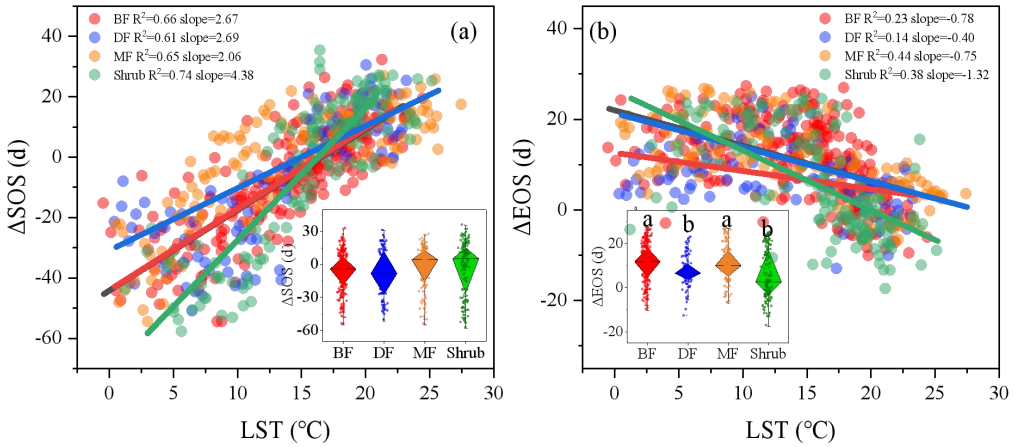

Figure 6. The relation between ΔSOS and ΔEOS with the LST across the 293 cities for different vegetation types, insert figures presented the comparison of averaged phenology difference across the 293 cities. BF: Broad-leaf forest, CF: Coniferous forest, MF: Mixed forest, Shrubs: Bush wood.

3.3 Quantify the LST determined phenological sensitivity

In order to obtain LST determined phenological sensitivity, the T in the first-order derivatives curves shown in Figures 5c and 5d was translated to LST considering the strong correlation between T and LST (Figure S4). Three distinct LST thresholds were identified: phenological date stabilization thresholds, urban-rural disparity reversal thresholds, and phenological sensitivity saturation thresholds. Specifically, phenological date stabilization and urban-rural disparity reversal occur at LST = 12 ℃ (SOS) / 18.5 ℃ (EOS), while phenological sensitivity saturates at LST = 12.5 ℃ (SOS) / 4 ℃ (EOS). Based on the first-order derivatives, we identified the specific thresholds for phenological sensitivity. We observed that when background LST exceeded 12.5 ℃ for spring and 4 ℃ for autumn, the temperature sensitivity (Rt) began to significantly weaken. This indicates a saturation of the physiological response rate, even though the absolute urban-rural difference (ΔSOS/ΔEOS) might still persist until higher temperatures are reached.

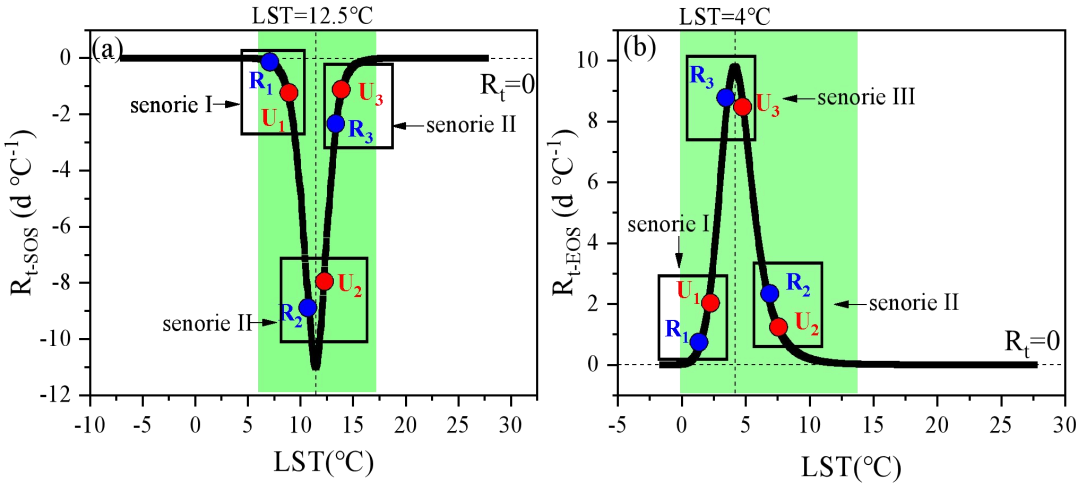

Figure 7. Schematic diagram for the three scenarios that likely occurred in the urban (red dots) and rural regions (blue dots) for SOS (I: $LST_{R1} < LST_{U1} < 12.5$ ℃; II: 12.5 ℃ $< LST_{R2} < LST_{U2}$; III: $LST_{R3} < 12.5$ ℃ $< LST_{U3}$) and EOS (I: $LST_{R1} < LST_{U1} < 4$ ℃; II: 4 ℃ $< LST_{R2} < LST_{U2}$; III: $LST_{R3} < 4$ ℃ $< LST_{U3}$).

Scenario I: when LST was less than 12.5 ℃ (4 ℃) for SOS (EOS), an increased LST was associated with heightened temperature sensitivity, resulting in urban regions (U_1) exhibiting higher sensitivity than rural regions (R_1) (Figure 5).

Scenario II: when LST exceeded 12.5 ℃ (4 ℃) for SOS (EOS), there was a weakened temperature sensitivity as LST increased, leading to urban regions (U_2) demonstrating higher sensitivity than rural regions (R_2) (Figure 5).

Scenario III: when urban LST surpassed 12.5 ℃ (4 ℃) while rural LST remained below 12.5 ℃ (4 ℃), the difference in sensitivity between urban and rural regions was inconclusive.

3.4 Phenology response to aridity

When the phenological responses were fitted to the AI, $R_{t\text{-}SOS}$ and ΔSOS were positively related to AI (Figure 8). It was noted that when AI < 1.7, there was a decrease in absolute $R_{t\text{-}SOS}$ with increasing AI, indicating that heightened aridity weakened the temperature sensitivity of SOS. Conversely, when AI > 1.7, most urban areas exhibited positive $R_{t\text{-}SOS}$ (resulting in delayed SOS), with higher AI values corresponding to greater $R_{t\text{-}SOS}$, suggesting that severe drought conditions adversely delay the onset of SOS.

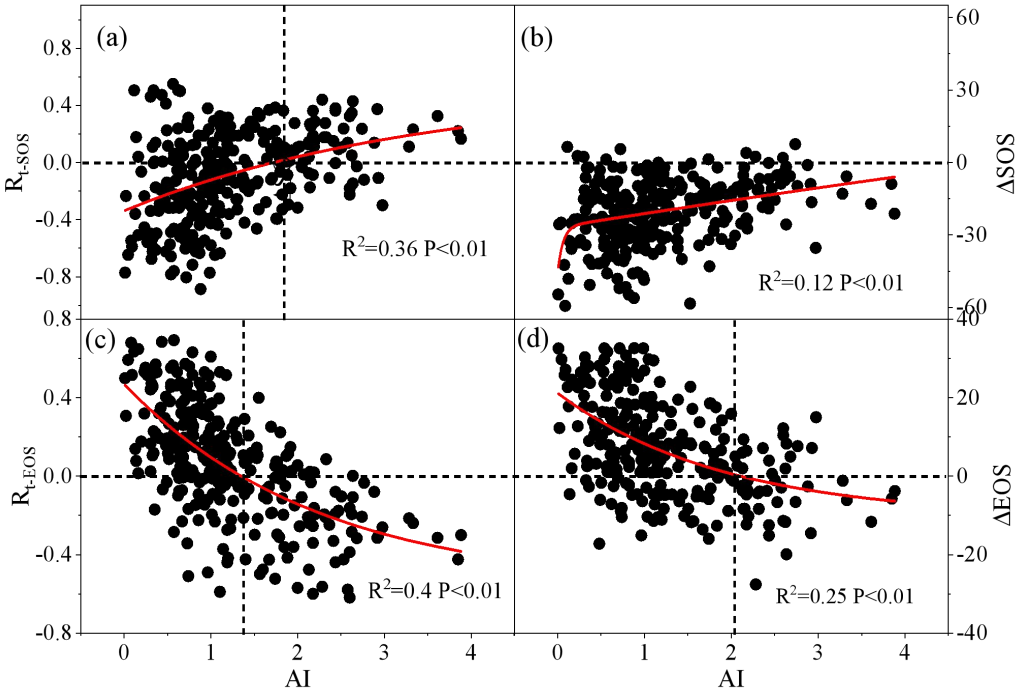

Figure 8. The AI determined phenological sensitivity and urban-rural difference. When the phenological responses were fitted to the AI, Rt-SOS and ΔSOS were positively related to AI.

While $R_{t\text{-}EOS}$ and ΔEOS were fitted against AI, a negative relation was observed. For $R_{t\text{-}EOS}$, when AI < 1.4, most of the $R_{t\text{-}EOS}$ was positive, and decreased with AI, i.e., the enhanced drought will offset the benefit of urban warming on the delayed EOS. When AI > 1.4, most cities shared a negative $R_{t\text{-}EOS}$, and the higher AI values corresponded to more negative $R_{t\text{-}EOS}$. I.e., extreme drought will lead to passive warming effects on EOS. It is noted that the negative ΔEOS tended to appear when AI > 2.

AI has been observed to advance ΔSOS and hasten ΔEOS across 293 cities, with this pattern holding true for all four vegetation types (Figure 9). Notably, ΔSOS in CF showed less sensitivity to AI influences than the other vegetation types. Both BF and MF demonstrated lower sensitivities to AI for both ΔSOS and ΔEOS, as compared to shrublands.

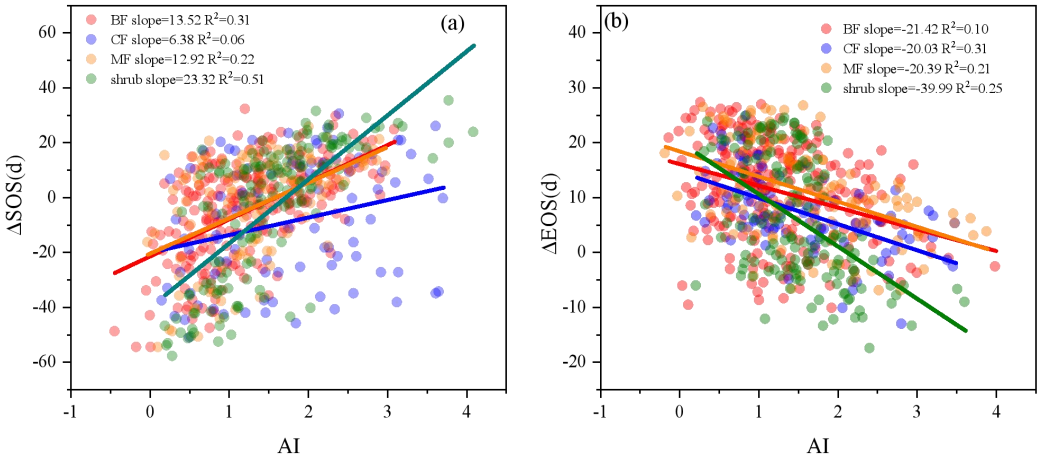

Figure 9. Relationships between AI and urban-rural phenological differences (ΔSOS, ΔEOS) across different vegetation types.

Panel (a): Scatter plot of ΔSOS versus AI with linear regression fits for each vegetation type.

Panel (b): Scatter plot of ΔEOS versus AI with linear regression fits for each vegetation type.

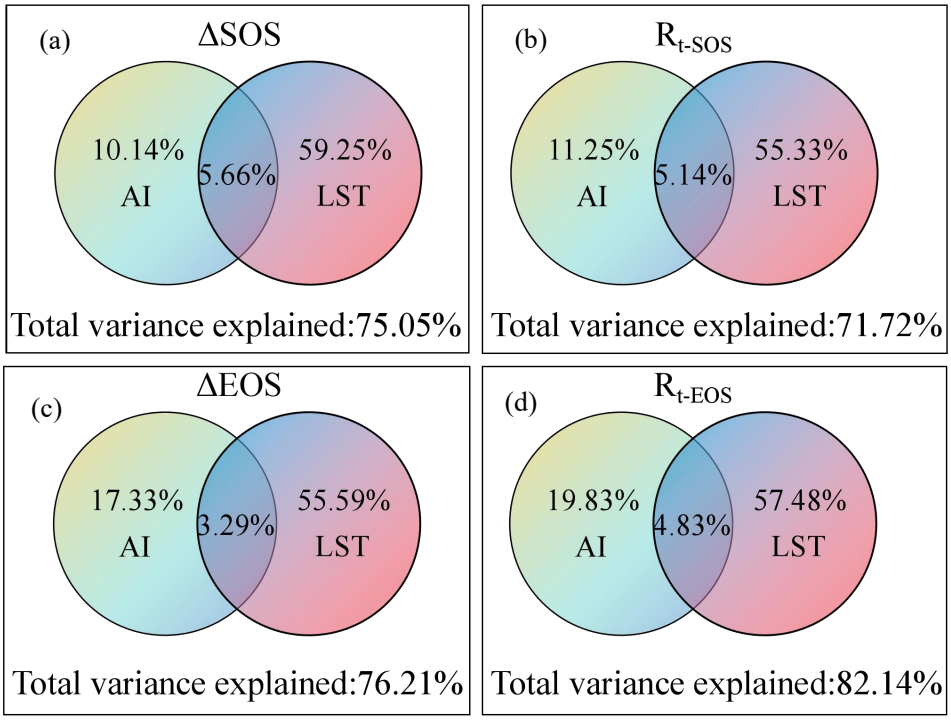

Figure 10. Venn diagrams illustrating the relative contributions of AI and LST to ΔSOS, ΔEOS, $R_{t\text{-}SOS}$, and $R_{t\text{-}EOS}$ across 293 Chinese cities.Note: Values in each section represent the percentage of variance independently explained by AI or LST and their

shared explanatory power in the overlapping region, and the total variance explained by both factors is labeled below each panel.

To further quantify the individual and combined contributions of LST and AI to phenological variations, a variance decomposition analysis was conducted (Legendre & Legendre, 2012; Figure 10). The Venn diagram revealed that AI and LST explained 75.05%, 71.72%, 76.21%, 82.14% for ΔSOS, ΔEOS, $R_{t\text{-}SOS}$, $R_{t\text{-}EOS}$ respectively (Figure 10), and LST always had more contributions for these phenology indicators. Besides, the interaction effect of LST and AI ranged from 3.29% to 5.66%.

4. Discussion

4.1 Overall urbanization effects on plant phenology in China

Our multi-city assessment confirms a predominant urban-rural phenological divergence across China, characterized by advanced SOS and delayed EOS within a concentrated 10-km urbanization footprint. This consistent spatial pattern validates that urban warming acts as a primary driver of phenological shifts. Beyond mere thermal forcing, this convergence across 293 cities reflects the profound impact of urban microclimates on plant life cycles. The observed 10-km threshold is particularly significant as it suggests a localized but intense ecological footprint that necessitates specialized urban greening management strategies, especially in high-density northern cities where these shifts are most pronounced.

Spatially, the pronounced north-south gradient in ΔSOS and ΔEOS across China, as shown in Figure 2, closely mirrors the spatial pattern of LST, reflecting the far stronger temperature sensitivity of vegetation phenology in northern regions relative to the south. This finding aligns with and supports previous research documenting greater phenological shifts in northern areas (Jia et al., 2021; Yang et al., 2025), and further highlights that background climate acts as a key modulator of urban phenological impacts. The more pronounced urban warming effects observed in coastal provinces relative to inland cities (Figure 2) likely stem from the buffering

effect of maritime climate on seasonal temperature constraints, which interacts with urban heat islands to amplify urban-rural phenological divergence. Moreover, the strong correlations between ΔSOS/ΔEOS, temperature sensitivity indicators ($R_{t\text{-}SOS}$ and $R_{t\text{-}EOS}$), LST, and AI, as presented in Figure 3, confirm that background temperature and aridity are critical drivers shaping the magnitude of urbanization-induced phenological shifts across the 293 cities, rather than just passive correlates, validating the core hypothesis of this study.

It is noted that the pattern of urban warming's benefit on the vegetation phenology was consistent among the four vegetation types (Figure S2). This consistency could be attributed to the ecological convergence of plants coexisting in shared local habitats within each city (Wang et al., 2016). Ecologically, the consistent 10-km effective footprint validates that urban environments function as distinct microclimatic 'islands.' This spatial boundary conceptually highlights that urban ecological engineering and greening strategies must account for highly localized, rather than regional, thermal forcings.

4.2 Background temperature related phenological response variance

When we quantified phenological responses to temperature across the climatic gradient, clear logistic trends were observed for both SOS and EOS (Figure 5). Consistent with this logistic trajectory, we observed that in urban areas, the growth rate for SOS/EOS began to plateau when temperatures exceeded 4 ℃/6 ℃, respectively (Figure 5). Taking into account the significant correlation between LST and T (Figure S4), we could also anticipate a diminished sensitivity in phenology with higher LST (Figure 7). These findings lend credibility to the "saturation" effect hypothesis, suggesting that the accelerating influence of warmth on vegetation phenology reported in earlier studies has its limits (Badeck et al., 2004; Li et al., 2021). Indeed, plants in the southern region exhibit not just a dampened phenological response but also a decelerated growth rate when faced with increasing temperatures (Li et al., 2021; Büntgen et al., 2019). As illustrated by the first-order derivatives in

Figure 5c and 5d, the phenological sensitivity to temperature does not increase linearly, but peaks at T=4 ℃ for SOS and T=6 ℃ for EOS before rapidly declining. Specifically, the stabilization of urban SOS at 101.3 days and rural SOS at 129.7 days when LST is low (Figure 4a) further demonstrates that plants reach a mandatory physiological threshold that cannot be bypassed by additional thermal forcing. Collectively, these results highlight that threshold- based nonlinear models rather than simple linear relationships are more suitable for predicting phenological responses under scenarios of continuous environmental warming, especially in urban settings. Conceptually, these saturation thresholds challenge the traditional linear paradigm of 'warming-driven phenological advancement'. By identifying explicit thermal boundaries, our framework establishes that the physiological capacity of urban vegetation to capitalize on UHI warming is strictly finite.

The observation of temperature saturation for the SOS in our study likely stems from the chilling requirements for vernalization (Kim et al., 2009; Hanninen et al., 2019). Typically, vegetation needs to undergo a period of exposure to low chilling temperatures to break dormancy. This mechanism is consistent with our spatial observations in Figure 2a, where cities in lower latitudes (warmer regions) exhibit significantly smaller ΔSOS values. This suggests that in these warmer territories, the higher background LST may fail to satisfy the necessary chilling requirements, leading to the diminished phenological sensitivity we quantified in Figure 3. Moreover, an earlier onset of greening increased the risk of damage from freezing events, posing a survival threat to the plants (Duan et al., 2011; Wang et al., 2015). This phenomenon explains the delayed SOS in approximately 16% of the cities under study, mainly distributed in low-latitude regions (Figure 4).

Regarding the EOS, a moderate increase in temperature could enhance the activities of photosynthetic enzymes (Shi et al., 2014), slow down the degradation of chlorophyll (Fracheboud et al., 2009), reduce the risk of frost exposure in autumn, and increase the potential for growth and photosynthetic production, ultimately promoting the extension of the growing season. While the benefits of increased temperature can be offset by the negative impacts of heat waves and excessive thermal stress (Mathur

et al., 2014). Our data in Figure 5b and 5d provides direct evidence for this: when preseason temperature (T) exceeds 15 ℃, a decreasing trend for EOS is observed. This aligns with the intersection points identified in Figure 4c and 4d at LST=18 ℃, where the urban-rural phenology difference reverses, confirming that excessive heat in urban centers triggers premature leaf senescence rather than further delaying it. In fact, when T > 15 ℃, EOS tends to be reduced, with an increased sensitivity to temperature changes (Estiarte & Penuelas, 2015; Figure 5b).

Despite the existence of "saturation" effects, lower background temperatures do not necessarily correspond to higher phenological sensitivity (Figure 4b, c). For SOS, when T < 4 ℃, the phenological sensitivity approached zero with decreased T (Figure 4c), which led to a stable SOS of 120d (Figure 5a, c). In fact, phenological events such as bud burst could not be triggered when high forcing temperatures threshold (cumulative temperature) was not fully provided (Hanninen et al., 2019). For EOS, when T > 6 ℃, the increased T sensitivity will produce more EOS advancement in the warmer regions. This reversal may be associated with abscisic acid synthesis induced by low temperatures, which accelerated the progress of defoliation.

Beyond thermal controls alone, our findings regarding the aridity-driven modulation of phenological responses provide a critical geographic context that complements previous observations. While earlier studies primarily emphasized thermal forcing as the dominant driver of urban phenology (Meng et al., 2020), our results demonstrate AI acts as a significant 'environmental filter' that can override or even reverse warming benefits. As shown in Figure 8 and 10, the high explanatory power of AI (up to 17.33% for ΔEOS) suggests that in water-limited regions of Northern and Western China, the physiological stress induced by drought prevents plants from utilizing the additional heat provided by the Urban Heat Island (UHI) effect. This phenomenon is consistent with the 'resource limitation' theory, where plant development is constrained by the most limiting resource (water; Harpole et al., 2011), regardless of optimal temperatures. Compared to coastal cities where water is abundant, the weakened warming benefits in arid inland cities highlight the need for regionally-differentiated urban irrigation strategies to maintain ecological productivity.

However, when LST<12.5 ℃, warming regions would have higher urban-rural difference of $\Delta R_{t\text{-}SOS}$, which contradicted the weakened urban-rural difference of $\Delta R_{t\text{-}SOS}$ raised in the previous study. For EOS, the warming benefits only occurred when 0<LST<18 ℃. Moreover, the weakened sensitivity was only detected in the LST interval of LST>4 ℃. The conclusions of weakened $\Delta R_{t\text{-}SOS}$ and $\Delta R_{t\text{-}EOS}$ in the USA may be due to their LST ranges was mostly falling in the ranges of 8 ℃-22 ℃.

4.3 AI related phenological response variance

In addition to background temperature (LST), the aridity index (AI) also drives significant spatial variation in urban-rural phenological disparities (ΔSOS, ΔEOS). Spatially, the coastal cities experienced more benefits from the urban warming (Figure 2). Our statistical decomposition in Figure 10 further elucidates this aridity-driven modulation, showing that AI and LST together explain over 75% of the variance in ΔSOS and ΔEOS. Notably, the fact that AI explains 17.33% of the variation in ΔEOS (Figure 10c) supports our inference that water availability is a critical limiting factor in autumn. This is further substantiated by the positive correlation between ΔSOS and AI in Figure 8b, which quantifies how increasing aridity progressively offsets the advanced green-up typically induced by urban warming. These results highlight that the warming benefits on the vegetation phenology will be weakend in those drought dominated regions. In fact, the delayed SOS was already proved in the previous studies (Ji et al., 2021; Yu et al., 2003).

Water deficit inhibits leaf growth via chemical signals (Knauer et al., 2017), and urbanization exacerbates drought stress (Zhang et al., 2019; Pollastrini et al., 2019), further weakening or even reversing the positive effects of urban warming on phenology. Besides, in water-stressed region, temperatures are already close to the optimum for photosynthesis, thus less benefits will be expected (Penuelas et al., 2004). The weakened temperature sensitivity in drought cities will certainly lead to less extension of growth season.

While it is noted that the influence of AI on the autumn phenology response was

higher than that on the spring phenology response (Figure 10). During spring leaf development, plants may use water stored in their bodies to support the growth of new leaves (Shi et al., 2023). Supporting evidence comes from the synchronous between plant water storage and leaf sprout for the boreal and temperate forests (Tian et al., 2018). In this case, the external water supply may have relatively little demand on the plant during the leaf development period, especially in some wetter areas. Comparatively, in summer and autumn, the transpiration of plants is larger, and the demand for water is strong (Wu et al., 2022), so the influence of drought degree on plant phenology will be more prominent. The overarching ecological implication here is a profound vulnerability: as background climates dry under global change, the compounding stress of UHI and background aridity may lead to 'phenological compression.' In arid urban ecosystems, this moisture deficit effectively neutralizes the anticipated carbon sequestration benefits of thermally extended growing seasons, rendering them highly sensitive to future climate extremes.

4.4 Phenological response variation among different vegetation types

The phenological response to LST and AI varies significantly across vegetation types, reflecting the influence of distinct ecological strategies. Our results (Figure 6 and 9) demonstrate that Shrublands are the most sensitive to both warming and aridity, likely due to their opportunistic resource utilization strategy and higher leaf turnover rates (Xiong et al., 2024). In contrast, Coniferous Forests exhibited a muted response to both drivers (Malla et al., 2023). While our analysis relies on broad land-cover categories and does not directly measure species-specific functional traits, these discrepancies likely reflect generalized divergent ecological strategies among the vegetation groups.

This insensitivity is substantiated by our AI-sensitivity analysis (Figure 9a), suggesting that the conservative hydraulic traits of conifers — such as needle morphology and lower stomatal conductance (Sperry et al., 2002; McAdam, 2013) — act as a buffer against the "aridity-driven inhibition" that more severely affects

broad-leaf species. Based on generalized ecological principles, this might be associated with typical drought-resistant adaptations found in many conifers (e.g., needle morphology and stricter stomatal control), which could limit the potential positive impact of warming on their phenology. In contrast, the heightened sensitivity of shrublands observed in our dataset aligns with literature suggesting more opportunistic resource utilization strategies in shrubs (Xiong et al., 2024).

By considering these functional differences, our study provides a more nuanced understanding of urban ecosystem resilience, suggesting that urban greening programs should prioritize drought-resistant coniferous or mixed forest structures in regions where the warming-saturation effect is most pronounced. However, we note that these functional interpretations remain broad generalizations; future studies incorporating field-based, species-level trait measurements are required to mechanistically validate these large-scale categorical patterns. Recognizing these trait-mediated responses is a crucial conceptual step for urban forestry. It indicates that building climate-resilient urban ecosystems requires shifting from generic greening to deploying specific functional traits—such as the conservative hydraulic strategies of conifers—to buffer against the coupled heat-aridity saturation effects.

5. Conclusion

Our study utilized remote sensing data to investigate the impact of urbanization on vegetation phenology across 293 Chinese cities from 2010 to 2020. Urban heat islands consistently advanced the start of growing season (SOS) by 12.06 days and delayed the end of growing season (EOS) by 9.86 days relative to rural areas. However, the magnitude of these shifts varied markedly with background land surface temperature (LST) and aridity index (AI), indicating that urban warming benefits are not universally distributed but are constrained by local climatic context.

We identified a non-linear "saturation effect" in phenological sensitivity to urban warming. Temperature sensitivity peaked at 4 °C (spring) and 6 °C (autumn), and weakened significantly beyond saturation thresholds of 12.5 °C for SOS and 4 °C for

EOS. Within the effective ranges of 3.5–17.5 °C (SOS) and 0–18 °C (EOS), urban warming exerted pronounced positive effects on phenological shifts; outside these ranges, sensitivity approached zero. Notably, extreme high temperatures reversed the beneficial effects for EOS, causing weakly delayed or even advanced senescence in warm urban regions.

Aridity emerged as a critical negative regulator of warming benefits. Across most AI ranges, increasing aridity attenuated the positive effects of UHI on both SOS and EOS. Within the intermediate aridity band of $1.4 < AI < 2.0$, warming benefits were entirely reversed. Consequently, coastal cities with lower AI exhibited substantially larger urban-rural phenological disparities than arid inland cities, where coupled heat-aridity stress compressed the effective growing season.

Collectively, these findings challenge the linear assumption that urban warming universally extends the growing season. Instead, they demonstrate that phenological responses to UHI are bounded by finite physiological limits and modulated by water availability. For urban ecological planning, our results imply that greening strategies must be climate-specific: drought-resistant vegetation structures should be prioritized in arid regions where saturation occurs at lower thermal thresholds, whereas coastal and northern cities can more effectively harness UHI benefits for growing season extension. Future research incorporating species-level functional traits and process-based phenology models will be essential to refine these thresholds and project urban ecosystem dynamics under continued global warming.

6. Author contributions: CRediT

Cui Shufen: Conceptualization, Methodology;

Zhang Zhenzhen: Data curation, Writing - Original draft preparation;

Hu Xinxin: Methodology, Formal analysis, Validation, Writing - review & editing;

Zhang Yongqi: Visualization, Investigation;

Sun Liheng, Wu Chaofan and Lin Xingwen: Supervision; Zhang Zhaoyang, Chen Yuanjian and Wen Qingqing: Software, Validation.

7. Data availability statement

The data that support the findings of this study are available in those public domain resources that listed in the table 1.

8. Competing interests

The authors declared that the research was conducted in the absence of any commercial or financial relationships that could be construed as a potential conflict of interest.

9. Acknowledgements

We appreciate the valuable suggestions from the Associate and anonymous reviewers, which substantially improved this manuscript. We also acknowledge the computing support provided by our university and the members of our research group for their assistance throughout this work.

10. Funding

This study was supported by "Department of science and technology of Zhejiang Province in China, 'Pioneer' and 'Bellwethers' R & D projects, grant number 2022C03119".

References

Angilletta, M. J. (2009). Thermal Adaptation: A Theoretical and Empirical Synthesis. Oxford: Oxford University Press.

Badeck, F.-W., Bondeau, A., Böttcher, K., Doktor, D., Lucht, W., Schaber, J. and Sitch, S. (2004). Responses of spring phenology to climate change. New Phytologist. **162,** 295-309.

Buyantuyev, A., & Wu, J. (2012). Urbanization diversifies land surface phenology in arid

environments: Interactions among vegetation, climatic variation, and land use pattern in the Phoenix metropolitan region, USA. Landscape and Urban Planning. **105,** 149-159.

Büntgen, U., Krusic, P.J., Piermattei, A., Coomes, D.A., Esper, J., Myglan, V.S., Kirdyanov, A.V., Camarero, J.J., Crivellaro, A., Körner, C. (2019). Limited capacity of tree growth to mitigate the global greenhouse effect under predicted warming. Nature Communications. **10,** 2171.

Cai, Z., Jönsson, P., Jin, H., & Eklundh, L. (2017). Performance of smoothing methods for reconstructing NDVI time-Series and estimating vegetation phenology from MODIS Data. Remote Sensing. **9,** 1271.

Čehulić, I., Sever, K., Katičić Bogdan, I., Jazbec, A., Škvorc, Ž., & Bogdan, S. (2019). Drought Impact on Leaf Phenology and Spring Frost Susceptibility in a Quercus robur L. Provenance Trial. Forests. **10,** 50.

Chmielewski, F.-M., & Rötzer, T. (2001). Response of tree phenology to climate change across Europe. Agricultural and Forest Meteorology. **108,** 101-112.

Cong, N., Piao, S., Chen, A., Wang, X., Lin, X., Chen, S., Han, S., Zhou, G., Zhang, X. (2012). Spring vegetation green-up date in China inferred from SPOT NDVI data: A multiple model analysis. Agricultural and Forest Meteorology. **165,** 104-113.

Dallimer, M., Tang, Z., Gaston, K. J., & Davies, Z. G. (2016). The extent of shifts in vegetation phenology between rural and urban areas within a human-dominated region. Ecology and Evolution. **6,** 1942-1953.

Ding, H., Xu, L., Elmore, A. J., & Shi, Y. (2020). Vegetation phenology influenced by rapid urbanization of The Yangtze Delta region. Remote Sensing. **12,** 1783.

Doncaster, C. P. (2007). Structural Equation Modeling and Natural Systems. Fish and Fisheries, 8(4), 368-369.

Duan, J., Zhang, Q.-B., Lv, L., & Zhang, C. (2011). Regional-scale winter-spring temperature variability and chilling damage dynamics over the past two centuries in southeastern China. Climate Dynamics. **39,** 919-928.

Elvidge, C. D., et al. (2017). VIIRS night-time lights. International Journal of Remote Sensing, 38(21), 5860-5879.

790 Estiarte, M., & Penuelas, J. (2015). Alteration of the phenology of leaf senescence and fall
791 in winter deciduous species by climate change: effects on nutrient proficiency. Global
792 Change Biology. **21,** 1005-1017.
793 Fan, J., He, H., Hu, T., Zhang, P., Yu, X., & Zhou, Y. (2019). Estimation of landscape
794 pattern changes in BRICS from 1992 to 2013 using DMSP-OLS NTL images.
795 Journal of the Indian Society of Remote Sensing. **47,** 725-735.
796 Fracheboud, Y., Luquez, V., Bjorken, L., Sjodin, A., Tuominen, H., & Jansson, S. (2009).
797 The control of autumn senescence in European aspen. Plant Physiology. **149,**
798 1982-1991.
799 Gazal, R., White, M. A., Gillies, R., Rodemaker, E. L. I., Sparrow, E., & Gordon, L.
800 (2008). GLOBE students, teachers, and scientists demonstrate variable differences
801 between urban and rural leaf phenology. Global Change Biology. **14,** 1568-1580 .
802 Ge, W., Han, J., Zhang, D., & Wang, F. (2021). Divergent impacts of droughts on
803 vegetation phenology and productivity in the Yungui Plateau, southwest China.
804 Ecological Indicators. **127**, 107743.
805 Gow, L. J., Barrett, D. J., Renzullo, L. J., Phinn, S. R., & O'Grady, A. P. (2016).
806 Characterising groundwater use by vegetation using a surface energy balance model
807 and satellite observations of land surface temperature. Environmental Modelling &
808 Software. **80,** 66-82.
809 Grimm, N. B., Faeth, S. H., Golubiewski, N. E., Redman, C. L., Wu, J., Bai, X., & Briggs,
810 J. M. (2008). Global change and the ecology of cities. Science, 319(5864), 756-760.
811 Hanninen, H., Kramer, K., Tanino, K., Zhang, R., Wu, J., & Fu, Y. H. (2019). Experiments
812 are necessary in process-based tree phenology modelling. Trends in Plant Science. **24,**
813 199-209.
814 Harpole, W. S., Ngai, J. T., Cleland, E. E., et al. (2011). Nutrient co-limitation of primary
815 producer communities. Ecology Letters, 14(9), 852-862.
816 He, C., Gao, B., Huang, Q., Ma, Q., & Dou, Y. (2017). Environmental degradation in the
817 urban areas of China: Evidence from multi-source remote sensing data. Remote
818 Sensing of Environment. **193,** 65-75.
819 Jeong, S. J., Park, H., Ho, C. H., & Kim, J. (2019). Impact of urbanization on spring and

autumn phenology of deciduous trees in the Seoul Capital Area, South Korea. International Journal of Biometeorology. **63,** 627-637.

Ji, S., Ren, S., Li, Y., Dong, J., Wang, L., Quan, Q., & Liu, J. (2021). Diverse responses of spring phenology to preseason drought and warming under different biomes in the North China Plain. Science of the Total Environment. **766,** 144437.

Jia, W., Zhao, S., Zhang, X., Liu, S., Henebry, G. M., & Liu, L. (2021). Urbanization imprint on land surface phenology: The urban-rural gradient analysis for Chinese cities. Global Change Biology. **27,** 2895-2904.

Jönsson, P., & Eklundh, L. (2004). TIMESAT—a program for analyzing time-series of satellite sensor data. Computers & Geosciences, 30(8), 833-845.

Kang, X., Hao, Y., Cui, X., Chen, H., Huang, S., Du, Y., Li, W., Kardol, P., Xiao, X., Cui, L. (2016). Variability and changes in climate, phenology, and gross primary production of an Alpine wetland ecosystem. Remote Sensing. **8,** 391.

Ketola, T., & Kristensen, T. N. (2017). Experimental approaches for testing if tolerance curves are useful for predicting fitness in fluctuating environments. Frontiers in Ecology and Evolution. **5,** 129.

Kim, D. H., Doyle, M. R., Sung, S., & Amasino, R. M. (2009). Vernalization: winter and the timing of flowering in plants. Annual Review of Cell and Developmental Biology. **25,** 277-299.

Knauer, J., Zaehle, S., Reichstein, M., Medlyn, B. E., Forkel, M., Hagemann, S., & Werner, C. (2017). The response of ecosystem water-use efficiency to rising atmospheric CO 2 concentrations: sensitivity and large-scale biogeochemical implications. New Phytologist. **213,** 1654-1666.

Legendre, P., & Legendre, L. (2012). Numerical Ecology (3rd ed.). Amsterdam: Elsevier.

Li, K., Wang, C., Sun, Q., Rong, G., Tong, Z., Liu, X., & Zhang, J. (2021). Spring phenological sensitivity to climate Change in the northern hemisphere: comprehensive evaluation and driving force analysis. Remote Sensing. **13,** 1972.

Malla, R., Neupane, P. R., & Köhl, M. (2023). Climate change impacts: Vegetation shift of broad-leaved and coniferous forests. Trees, Forests and People. **14,** 100457 .

Mathur S., Agrawal D., Jajoo A. (2014). Photosynthesis: response to high temperature

stress. Journal of Photochemistry and Photobiology B: Biology. **137,** 116-126.

McAdam, B. S. A. M. J. P. P. (2013). Abscisic acid mediates a divergence in the drought response of two conifers. Plant physiology. **162,** 1370-1377.

Meng, L., Mao, J., Zhou, Y., Richardson, A.D., Lee, X., Thornton, P.E., Ricciuto, D.M., Li, X., Dai, Y., Shi, X., Jia, G. (2020). Urban warming advances spring phenology but reduces the response of phenology to temperature in the conterminous United States. Proceedings of the National Academy of Sciences of the United States of America. **117,** 4228-4233.

Mu, Q., Zhao, M., & Running, S. W. (2011). Improvements to a MODIS global terrestrial evapotranspiration algorithm. Remote Sensing of Environment, 115(8), 1781-1800.

Pablos, M., Martínez-Fernández, J., Piles, M., Sánchez, N., Vall-llossera, M., & Camps, A. (2016). Multi-temporal evaluation of soil moisture and land surface temperature dynamics using in situ and satellite observations. Remote Sensing. **8,** 587.

Peng, J., Wu, C., Zhang, X., Wang, X., & Gonsamo, A. (2019). Satellite detection of cumulative and lagged effects of drought on autumn leaf senescence over the Northern Hemisphere. Global Change Biology. **25,** 2174-2188.

Peng, S. (2020). 1-km monthly precipitation dataset for China (1901-2021). Retrieved from: https://dx.doi.org/10.5281/zenodo.3185722.

Penuelas, J., Gordon, C., Llorens, L., Nielsen, T., Tietema, A., Beier, C., ... & Gorissen, A. (2004). Nonintrusive field experiments show different plant responses to warming and drought among sites, seasons, and species in a north–south European gradient. Ecosystems. **7,** 598-612.

Piao, S., Fang, J., Zhou, L., Ciais, P., & Zhu, B.(2006). Variations in satellite-derived phenology in China's temperate vegetation. Global Change Biology. **12,** 672-685.

Pinheiro, J. C., & Bates, D. M. (2000). Mixed-Effects Models in S and S-PLUS. Springer.

Pollastrini, M., Puletti, N., Selvi, F., Iacopetti, G., & Bussotti, F. (2019). Widespread crown defoliation after a drought and heat wave in the forests of Tuscany (Central Italy) and their recovery—A case study from summer 2017. Frontiers in Forests and Global Change. **2**.

Qiao, Z., Tian, G., & Xiao, L. (2013). Diurnal and seasonal impacts of urbanization on the

urban thermal environment: A case study of Beijing using MODIS data. ISPRS Journal of Photogrammetry and Remote Sensing. **85,** 93-101.

Qiu, T., Song, C., & Li, J. (2017). Impacts of urbanization on vegetation phenology over the past three decades in Shanghai. China. Remote Sensing. **9,** 970.

Qiu, T., Song, C., Zhang, Y., Liu, H., & Vose, J. M. (2020). Urbanization and climate change jointly shift land surface phenology in the northern mid-latitude large cities. Remote Sensing of Environment. **236,** 111477.

Rustad, L., Campbell, J., Marion, G., Norby, R., Mitchell, M., Hartley, A., Cornelissen, J., Gurevitch, J., Gcte, N. (2001). A meta-analysis of the response of soil respiration, net nitrogen mineralization, and aboveground plant growth to experimental ecosystem warming. Oecologia. **126,** 543–562.

Sage, R.F. and Kubien, D.S. (2007). The temperature response of C3 and C4 photosynthesis. Plant. Cell & Environment. **30,** 1086-1106.

Shi, C., Sun, G., Zhang, H., Xiao, B., Ze, B., Zhang, N., & Wu, N. (2014). Effects of warming on chlorophyll degradation and carbohydrate accumulation of Alpine herbaceous species during plant senescence on the Tibetan Plateau. PLoS OnE. **9,** e107874.

Shi, W., Li, J., Zhan, H., Yu, L., Wang, C., & Wang, S. (2023). Relation between water storage and photoassimilate accumulation of neosinocalamus affinis with phenology. Forests. **14,** 531.

Sperry, J. S., Hacke, U. G., Oren, R., & Comstock, J. P. (2002). Water deficits and hydraulic limits to leaf water supply. Plant, Cell & Environment, 25(2), 251-263.

Tang, J. W., Korner, C., Muraoka, H., Piao, S. L., Shen, M. G., Thackeray, S. J., & Yang, X. (2016). Emerging opportunities and challenges in phenology: a review. Ecosphere. **7,** e01436.

Tian, F., Wigneron, J.-P., Ciais, P., Chave, J., Ogée, J., Peñuelas, J., Ræbild, A., Domec, J.-C., Tong, X., Brandt, M., Mialon, A., Rodriguez-Fernandez, N., Tagesson, T., Al-Yaari, A., Kerr, Y., Chen, C., Myneni, R.B., Zhang, W., Ardö, J., Fensholt, R. (2018). Coupling of ecosystem-scale plant water storage and leaf phenology observed by satellite. Nature ecology & Evolution. **2,** 1428-1435.

910 Wan, Z. (2008). New refinements and validation of the MODIS Land-Surface
911 Temperature/Emissivity products. Remote Sensing of Environment. **112**, 59-74 .
912 Wang, C., Cao, R., Chen, J., Rao, Y., & Tang, Y. (2015). Temperature sensitivity of spring
913 vegetation phenology correlates to within-spring warming speed over the Northern
914 Hemisphere. Ecological Indicators. **50,** 62-68.
915 Wang, C., Tang, Y., & Chen, J. (2016). Plant phenological synchrony increases under rapid
916 within-spring warming. Scientific Reports. **6,** 25460.
917 Wang, Z., Ma, R., Zhao, M., Wang, F., Zhang, N., & Si, H. (2020). NO and ABA
918 interaction regulates tuber dormancy and sprouting in Potato. Frontiers in Plant
919 Science. **11,** 311.
920 White, M.A., De Beurs, K.M., Didan, K., Inouye, D.W., Richardson, A.D., Jensen, O.P.,
921 O'Keefe, J., Zhang, G., Nemani, R.R., Van Leeuwen, W.J.D., Brown, J.F., De Wit, A.,
922 Schaepman, M., Lin, X., Dettinger, M., Bailey, A.S., Kimball, J., Schwartz, M.D.,
923 Baldocchi, D.D., Lee, J.T., Lauenroth, W.K. (2009). Intercomparison, interpretation,
924 and assessment of spring phenology in North America estimated from remote sensing
925 for 1982-2006. Global Change Biology. **15,** 2335-2359 .
926 Wu, C., Peng, J., Ciais, P., Peñuelas, J., Wang, H., Beguería, S., ... & Ge, Q. (2022).
927 Increased drought effects on the phenology of autumn leaf senescence. Nature
928 Climate Change. **12,** 943-949.
929 Wu, D., Zhao, X., Liang, S., Zhou, T., Huang, K., Tang, B., & Zhao, W. (2015). Time-lag
930 effects of global vegetation responses to climate change. Global change biology. **21,**
931 3520-3531.
932 Xiong, X., Wu, H., Wei, X., & Jiang, M. (2024). Contrasting temperature and light
933 sensitivities of spring leaf phenology between understory shrubs and canopy trees:
934 Implications for phenological escape. Agricultural and Forest Meteorology. **355,**
935 110144.
936 Yang, H., Zhang, Q., Zhang, S., et al. (2025). Joint control of urban expansion and climate
937 change on urban-rural vegetation phenology gradient in 31 cities of China. Frontiers
938 in Ecology and Evolution, 13, 1637210.
939 Yao, R., Wang, L., Huang, X., Guo, X., Niu, Z., & Liu, H. (2017). Investigation of

Urbanization effects on land Surface phenology in Northeast China during 2001–2015. Remote Sensing. **9,** 66.

Yu, F., Price, K. P., Ellis, J., & Shi, P. (2003). Response of seasonal vegetation development to climatic variations in eastern central Asia. Remote Sensing of Environment. **87,** 42-54.

Yuan, M., Zhao, L., Lin, A., Wang, L., Li, Q., She, D., & Qu, S. (2020). Impacts of preseason drought on vegetation spring phenology across the Northeast China Transect. Science of the Total Environment. **738,** 140297.

Zhang, X., Friedl, M. A., Schaaf, C. B., Strahler, A. H., & Schneider, A. (2004). The footprint of urban climates on vegetation phenology. Geophysical Research Letters. **31,** L12209.

Zhang, X., Friedl, M. A., & Schaaf, C. B. (2006). Global vegetation phenology from Moderate Resolution Imaging Spectro radiometer (MODIS): Evaluation of global patterns and comparison with in situ measurements. Journal of Geophysical Research: Biogeosciences. **111**.

Zhang, X., Chen, N., Sheng, H., Ip, C., Yang, L., Chen, Y., ... & Niyogi, D. (2019). Urban drought challenge to 2030 sustainable development goals. Science of the Total Environment. **693,** 133536.

Zheng, W., Liu, Y., Yang, X., & Fan, W. (2022). Spatiotemporal variations of forest vegetation phenology and its response to climate change in northeast China. Remote Sensing. **14,** 2909.

Zhou, D., Zhao, S., Zhang, L., & Liu, S. (2016). Remotely sensed assessment of urbanization effects on vegetation phenology in China's 32 major cities. Remote Sensing of Environment. **176,** 272-281.